ChemComm

FEATURE ARTICLE

View Article Online
View Journal | View Issue

Cite this: *Chem. Commun.*, 2024, **60**, 5790

Received 12th January 2024,
Accepted 22nd April 2024

DOI: 10.1039/d4cc00183d

rsc.li/chemcomm

Porous protein crystals: synthesis and applications

Alec Arthur Jones [a] and Christopher D. Snow *[ab]

Large-pore protein crystals (LPCs) are an emerging class of biomaterials. The inherent diversity of proteins translates to a diversity of crystal lattice structures, many of which display large pores and solvent channels. These pores can, in turn, be functionalized *via* directed evolution and rational redesign based on the known crystal structures. LPCs possess extremely high solvent content, as well as extremely high surface area to volume ratios. Because of these characteristics, LPCs continue to be explored in diverse applications including catalysis, targeted therapeutic delivery, templating of nanostructures, structural biology. This Feature review article will describe several of the existing platforms in detail, with particular focus on LPC synthesis approaches and reported applications.

1. Introduction

Proteins are well-suited as a substrate for material applications, due to their biocompatibility,[1] and structural diversity.[2] A variety of mesostructures emerge as a property of their constitutive nanostructures; these include protein nanoparticles,[3] nanocages,[4,5] hydrogels,[6] plate-like crystals and sheets,[7,8] and porous scaffolds.[9–11]

Porous materials, with their ability to host and transport guest molecules within their frameworks, have been explored in recent years for diverse scientific and industrial applications. Among these, large-pore protein crystals (LPCs) represent a distinctive class of crystalline materials characterized by a three-dimensional network of interconnected voids and channels. Large-pore protein crystals exhibit remarkable structural diversity compared with traditional nanomaterials, owing to the diversity of protein sequences found in nature. A typical bacterial protein sequence of 300 amino acids,[12] could have 20^{300} distinct amino acid sequences; assuming ~8 conformational degrees of freedom per residue,[13,14] the number of possible conformations extends to $\sim 1.72 \times 10^{661}$ theoretical conformations, effectively an infinite landscape of structural diversity. While most of these hypothetical structures would be unstable and any plausible structure would be restricted to

[a] *School of Biomedical Engineering, Colorado State University, Fort Collins, CO 80523-1301, USA. E-mail: christopher.snow@colostate.edu*
[b] *Department of Chemical and Biological Engineering, Colorado State University, Fort Collins, CO 80523-1301, USA*

Alec Arthur Jones

Alec A. Jones is an Anschutz Foundation fellow and PhD student in the School of Biomedical Engineering at Colorado State University. Prior to joining the Snow lab, he obtained his B.Sc. in biology at the University of South Carolina – Aiken in 2018, where he studied craniofacial skeletal development in zebrafish. His current research is focused on the development of porous protein microcrystals as delivery vectors for gene therapy, as catalytic scaffolds, and as a capture scaffold for viruses.

Christopher D. Snow

Prof. Christopher Snow received a B.S. degree in Chemistry from MIT in 2001 and his PhD in Biophysics from Stanford University in 2006. As a Howard Hughes fellow at Stanford, Dr Snow studied the biophysics of protein folding using distributed computing. He worked with Frances Arnold at Caltech from 2006–2011 as a Jane Coffin Childs Fellow and a KAUST Research Fellow. Since coming to Colorado State University in 2011, he has led a combined computation and experimental laboratory with a significant focus on the design, engineering, and applications of biomolecular crystals.

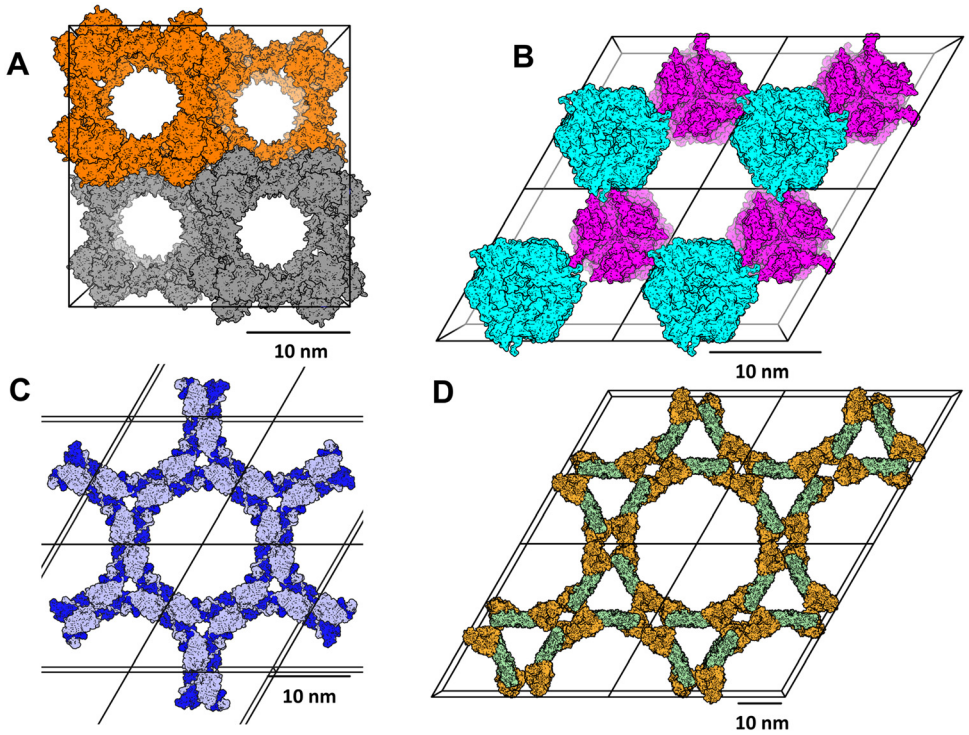

Fig. 1 Lattice structures for Protein Data Base entries (A) 4QCC, (B) 2INY, (C) 5W17, and (D) 2IOU, illustrating the diversity of porous nanostructures found in protein crystals. Pore diameters range from ~10 nm (2INY), up to ~30 nm (2IOU). Scale bar = 100 Å.

narrowly defined minima within this energy landscape, the number of stable structures is nevertheless vast. The ability of proteins to undergo genetic selection, along with the wholesale shuffling and recombination of domains[15] enables a realistic sampling of this landscape. The enormous diversity of protein structures (and functions) has sparked a growing interest in their potential applications as biomimetic scaffolds.

The unique architecture of protein crystals arises from the self-assembly of protein molecules into ordered, crystalline structures. Protein crystals typically contain a high surface area to volume ratio[16] with a well-defined lattice of interconnected pores. Pore diameters typically range from tens of Angstroms to greater than 10 nm (Fig. 1) with corresponding wide-ranging solvent content between 27% and 65%.[11,17–21] These solvent channels enable the accommodation of a wide array of guest molecules, from small ions to large biomolecules such as peptides, nucleic acids, and other proteins. Possessing solvent channels of sufficient size for guest macromolecule transport would be one characteristic of the LPC subset of protein crystals. The Matthews coefficient (V_M), defined as the fraction of crystal volume per unit of protein molecular weight (Å^3 Da^{-1}), is a useful parameter for specifying solvent content. More recent estimates on the distribution of V_M, based on reported crystallographic data, suggest that V_M of reported protein crystals is quite broad, from extremely high density (just over 1 Å^3 Da^{-1}, approximating tightly-packed spheres) to extremely low density in the case of LPCs (just below 10 Å^3 Da^{-1}).[22,23] Due to their high solvent content and void space, LPCs are also uniquely sensitive to dehydration, which typically results in contraction of the overall crystal structure. Dehydration can be achieved in a controlled manner by altering the relative humidity or osmolarity of the surrounding environment of the crystal.[24] While deformation of the nanostructure is often undesirable for material applications of LPCs, for structural investigations, crystals may be deliberately dehydrated to improve their diffraction resolution, although cracks or other broad morphological defects can potentially negate the improved diffraction limit.[25]

Understanding the formation mechanisms of LPCs is pivotal for their controlled synthesis. Crystallization of biomolecules is notably distinct from crystallizing small molecules, owing primarily to their increased molecular weight and complexity. The crystallization process involves an interplay of many factors, including protein concentration, pH, temperature, ionic strength, and the presence of precipitants and nucleating agents.[26] Proteins have additional considerations such as susceptibility to misfolding and ease of expression and purification. Recent advances in protein engineering and biophysical techniques have facilitated the rational design and optimization of LPCs.

Notably, while LPC growth is similar to the growth of other less porous protein crystals, a key distinguishing characteristic is that sufficiently large pores could allow building blocks throughout the crystal to exchange with solution. A candidate quantitative threshold for LPCs, therefore, would be any protein crystal with solvent channels of sufficient diameter to allow transport of the constituent crystal building blocks – in other words, LPCs may be defined as protein crystals whose pore

radius is at least twice the hydrodynamic radius of the constituent monomer. Precise nanopore sizes within a crystal lead to a sharp cutoff on transport depending on guest size. Accordingly, biomolecular crystals have been explored as molecular sieves for selective adsorption and separation of biomolecules.[27] The confined environment within LPCs also provides a unique platform for enzyme immobilization and colocalization, enhancing catalytic efficiency and stability.[28–30] Specific applications for LPCs that have been investigated include catalysis, templating of nanostructures, and targeted therapeutic delivery of bioactive compounds, all of which will be described in this review. This Feature Article will provide a broad overview of the current state of LPCs, with particular focus on their methods of synthesis and specific applications.

2. Synthesis methods

2.1. Control of size and morphology

Historically, protein crystallization has been most often used for the specific purpose of generating large, uniform crystals that are ideal for X-ray diffraction.[31] Due to their irregular shape and complex interactions with each other and the surrounding solvent, many proteins have a tendency to crystallize into structures which feature sizable solvent-filled cavities and pores. Multiple synthesis routes have been described for generating nanoporous scaffolds from proteins. The most commonly reported approach involves first growing the crystal using conventional methods, such as sitting- or hanging-drop vapor diffusion or batch crystallization. Vapor diffusion methods generally result in larger, fewer crystals, and are more suited towards generating crystals for X-ray diffraction. One common approach involves mixing concentrated protein stock with a high-ionic strength precipitant buffer (*e.g.* a buffered high-salt solution, such as sodium chloride or ammonium sulphate). The wells also contain a reservoir containing the undiluted precipitant solution. The wells are subsequently sealed, and water molecules diffuse through the vapor phase between the well solution and the droplet containing protein. Due to the lower salt concentration within the protein droplet, equilibrium between the droplet and the well results in a gradual net decrease in volume in the protein droplet. The resulting gradual increase in protein and salt concentration occurs slowly enough that nucleation proceeds very slowly, and metastable growth of crystals can begin immediately after nucleation (Fig. 2).

Batch crystallization is distinct from vapor diffusion in that both the protein and precipitant are mixed in a single volume, without any vapor-phase equilibration. At sufficiently high protein and precipitant concentrations, nucleation proceeds very rapidly, resulting in many smaller crystals. This approach is well-suited for generating a large number of small crystals, although it requires optimization to avoid issues such as excess protein aggregation. The "CJ" crystals used by our group, from a putative polyisoprenoid-binding protein from *Campylobacter jejuni* have been shown to possess very large solvent channels (>13 nm diameter), *via* X-ray diffraction[9] and atomic force microscopy.[32] We have frequently relied on batch crystallization to generate large quantities of small porous microcrystals for a variety of applications.

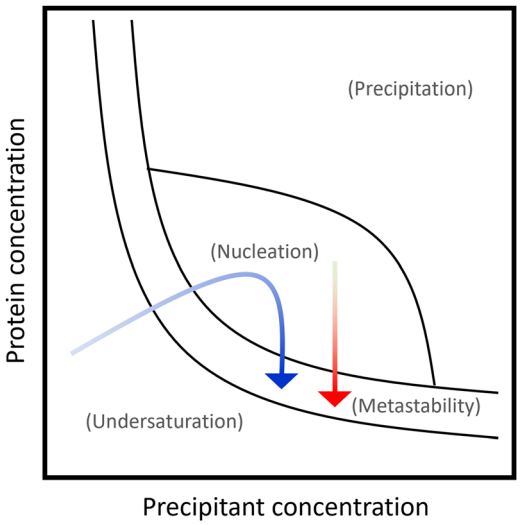

Fig. 2 Phase diagram showing the trajectory, over time, of protein and precipitant concentration for vapour diffusion (blue arrow) and batch crystallization (red arrow).

Methods for generating porous protein structures include growth of complete structures from constituent monomers ("bottom-up"), or crystal growth followed by disassembly into sub-structures, such as protein nanotubes or cages. While most of the systems described in this review conform to a bottom-up approach, a number of approaches that instead use the crystal form as a template have been described. For instance, Ueno and coworkers constructed a supramolecular nanotube assembly, by mutating a key interface residue (I149C) in RuBisCO from *Thermococcus kodakaraensis*.[33] After growth, the crystals were cross-linked in an oxidizing buffer for 24 hours; following cross-linking, the crystals were dissolved into their constituent nanotubes by soaking in an alkaline solution, and subsequently characterized *via* transmission electron microscopy.[33] Proposed applications of such tubular assemblies include templating of nanomaterials, as confinement within the tube enables size-restricted growth of inorganic materials like nanorods (a similar approach by the Ueno group is described in more detail in Section 3.3). Similar top-down strategies for synthesizing porous protein structures, specifically protein cages, have been employed by the Care group[34] and Hilvert group.[5]

Porous proteinaceous materials are not restricted to large proteins alone. Heinz-Kunert *et al.* constructed a porous peptide framework from a synthetic peptide building block.[35] The building block consisted of a simple α helix, containing rigid, planar, and highly aromatic bipyridyl residues extending from the N- and C-termini; the bipyridyl side chains can participate in π-stacking with neighbouring peptides, resulting in the formation of a porous lattice.[35] While this system is restricted to small-length peptides, the resulting scaffold shares the characteristic tunability of LPCs *via* amino acid substitutions, as evidenced by changes in molar uptake of Nile red in

response to substitutions at the pore-facing residues.[35] Similarly, cyclic peptide nanotubes (cPNTs) have received increasing attention in recent years for a number of applications, particularly for therapeutic delivery,[36,37] owing to their high biocompatibility and ease of synthesis. Similar to LPCs, cPNTs can be synthesized with a range of pore sizes,[38,39] in some cases as high as 2 μm in diameter.[40] Furthermore, a significant advantage of these systems is the ease with which they can be incorporated into the lipid bilayer of the plasma membrane.

Any discussion of LPC microcrystal synthesis would not be complete without consideration for production scale-up. Furthermore, synthesis of LPC microcrystals is unlike synthesis of conventional meso- and microporous scaffolds, insofar as it relies on a biologically derived building block, whereas more traditional systems, including mesoporous silica particles and other inorganic and polymer-based systems are traditionally composed of non-biologically derived substances. Scaled production of lysozyme nano- and microcrystals has been described using an oscillatory flow reactor,[41,42] in which control of size and crystal abundance is achieved *via* increased turbulent mixing. More critically, however, the necessity to express and purify a recombinant protein from a host organism results in a significant increase in both time and expense, compared with other porous nano- and microparticle scaffolds. One potential method of overcoming these obstacles involves overexpressing and crystallizing the scaffold protein *in vivo* or in living cells. Abe *et al.* from the Ueno group have observed crystallization of polyhedrin in insect cells (*S. frugiperda* and *B. mori*),[27] recapitulating earlier observations by Mori *et al.*[43] Similar *in vivo* crystallization approaches have been used for generating Cry3 crystals.[44] More recent work by the Ueno group describes a cell-free system for generating nanocrystals, by co-incubating template mRNA with wheat germ extract;[45] although these crystallization reactions were only performed at millilitre scales, this approach, similar to *in vivo* crystallization, obviates the need for downstream purification of the protein.

For most of the downstream applications described in this article, it is favourable to generate monodisperse crystals of very small sizes (ideally less than 5 μm in diameter). For this reason, many methods have been explored for generating nano- and microcrystals in large batches. Crystal size, as well as crystallization efficiency (defined as the ratio of crystallized protein to total protein) is influenced most heavily by protein concentration, followed by precipitant concentration, temperature, pH, and the presence of nucleating agents.[46]

The canonical methods for growing protein crystals include batch crystallization, microdialysis, and sitting- and hanging-drop vapor diffusion. While vapor diffusion is a preferred method for growing large crystals, droplet handling is typically impractical for generating many small crystals. Nevertheless, it can be useful in the context of studying the behaviour of LPCs at a visible scale. Within our group, thanks to the conserved nanostructure of both large and small crystals, we routinely predict the behaviour of smaller porous microcrystals from X-ray diffraction and fluorescence microscopy of larger crystals, which are easier to manipulate and observe.[11,47,48]

2.2. Enhancing crystal stability

Most crystals derived from biomolecules are susceptible to dissolution when transferred outside of their mother liquor.

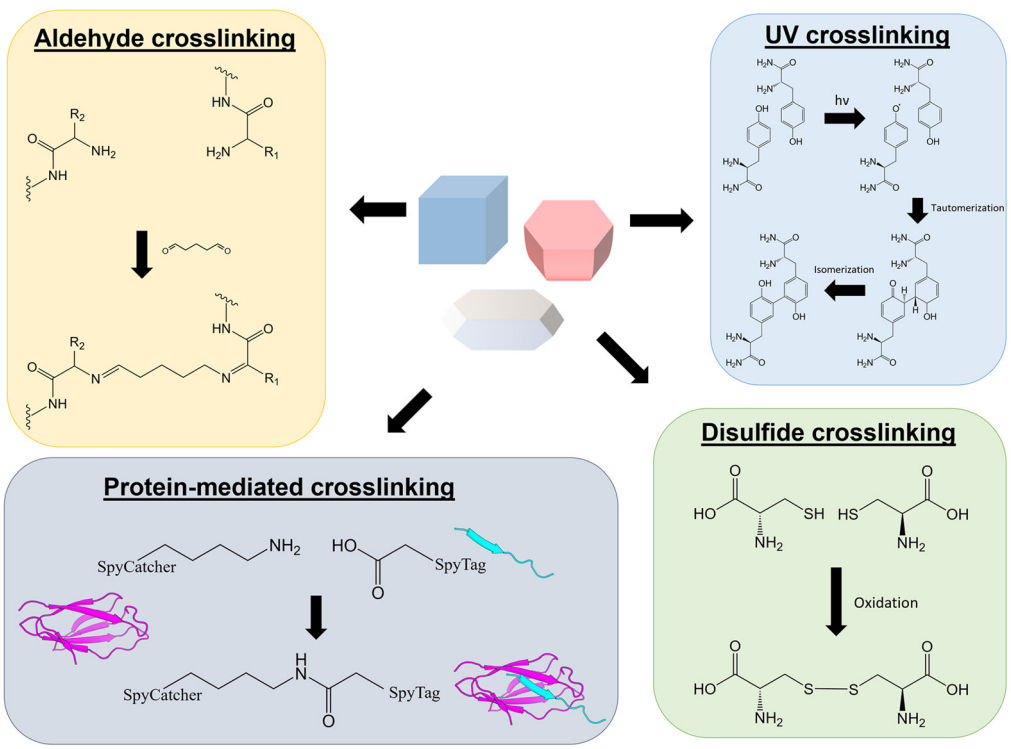

Fig. 3 An overview of the various reported methods for cross-linking PPCs, or stabilizing guest-crystal interactions, via covalent bonds.

Therefore, it is often necessary to chemically crosslink the crystals following growth and washing, to ensure that they retain their structural integrity following solvent exchange. Some rare protein crystals, such as crystals derived from the insecticidal, *Bacillus thuringiensis*-derived Cry toxins[44,49] do not require additional downstream cross-linking. S-layer proteins, which confer structural rigidity to the outer membrane of certain prokaryotic species, have also been shown to form highly stable two-dimensional porous crystals on the surface of living cells.[50–52]

Commonly reported methods for stabilizing protein crystals (Fig. 3) include chemical methods such as formaldehyde,[53] glutaraldehyde,[54,55] 1-ethyl-3-(3-dimethylaminopropyl)-carbodiimide,[56,57] and glyoxal.[58,59] Oxidation of proximal cysteines to promote the formation of disulfide bonds within LPCs is another well-established strategy.[60–62] While sortases[63–65] and SpyCatcher/SpyTag[66] have been well studied in the context of enzyme immobilization and installation of guests within or on scaffolds, these systems have been less characterized for their use in stabilizing the scaffold itself.

Solution exchange and downstream handling are potential challenges when cross-linking LPCs. In an ideal scenario, the crystals should be stabilized within their mother liquor immediately following or during growth, as downstream handling and washing steps and solution exchanges can result in mishandling and damaging of the crystals. Ultraviolet photocrosslinking is an alternative strategy for LPC stabilization that remains largely unexplored. UV excitation of tyrosine-rich proteins in the presence of strong oxidizers, such as Ru(II) complexes, results in the formation of reactive radical species which can subsequently form covalent bonds with neighbouring tyrosines.[67] Similar chemistries are believed to contribute to the mechanical strength of insect wings[68] and fibroin and keratin structures in Tussah silk.[69] Dityrosine crosslinking has been employed for other structure determination-based methods such as mass spectrometry[70,71] and NMR,[72] and has seen some use as a method for stabilizing protein films and nanoparticles.[73] At the same time, it should be noted that radical chemistry can result in the undesirable formation of free-radical species and unintended side reactions within the crystal; UV photocrosslinking is a common method for sterilization and inactivating enzymes *in vitro*.[74] For biochemically inert scaffolds however, the reduced handling and transfer steps may make UV-induced crosslinking an attractive strategy for stabilizing LPCs.

2.3. Validation

While this article has described some of the methods for generating LPCs, as well as stabilizing them outside of their mother liquor, it is worth noting that the methods for characterizing LPCs themselves are similarly diverse, and these depend in large part on the nature of the crystals themselves. Properties of interest include crystal size, porosity, dimensionality, and tolerance to desiccation. Many of the methods for studying the morphology and behaviour of LPCs overlap significantly with established techniques used in materials engineering, and structural and cell biology.

For small crystals, scanning electron microscopy (SEM) is often used to validate both the size and correct habit of porous microcrystals. For tiny crystals (<1 μm diameter), dynamic light scattering (DLS) is another technique used for size validation and has the additional benefit of being able to measure the surface zeta potential. The latter property is critical for ensuring that crystals are monodisperse in solution. DLS involves measuring the frequency in intensity of incident scattered light off of a sample over time, in order to build a correlation function that reveals the overall rate of diffusion of particles in a sample. Size determination, in turn, relies on the relationship between the diffusion coefficient (D) and the hydrodynamic radius (R_H) of a given particle, as described by the Stokes–Einstein equation:[75,76]

$$D = \frac{k_B T}{6\pi\eta R_H}$$

Regarding kinetics, crystal formation is commonly hypothesized to proceed in a two-step fashion – nucleation, followed by metastable growth.[77–79] Furthermore, the thermodynamics of crystal nucleation are believed to result in a two-step process – aggregation into protein-rich clusters, followed by phase transition into an ordered crystal structure (for this reason, nucleation is recognized as the rate-limiting step in microcrystal formation). The free energy associated with homogeneous nucleation (characteristic of batch crystallization) is dependent on the volume (bulk) free energy, solvent-accessible (interfacial) free energy, and the surface tension between the nucleus and surrounding solution.[80]

Because crystal nucleation is preceded by the formation of disordered liquid clusters, one of the challenges of using DLS to monitor crystal growth is its inability to distinguish between amorphous protein clusters and well-ordered nanocrystals. Fortunately, because crystalline materials demonstrate much higher form birefringence than amorphous aggregate, DLS can be used in combination with depolarized DLS (DDLS) in order to reliably distinguish nanocrystals from disordered aggregates, allowing for real-time monitoring of crystal formation.[81] The Chan group has also routinely used SEM and DLS on Cry3Aa crystals to validate their morphology and size.[10]

For direct evaluation of crystal porosity, transmission electron microscopy (TEM) is one of the more commonly reported methods.[82] Our group has used SEM to characterize the size and shape of LPC microcrystals, and atomic force microscopy (AFM) to characterize the pore surface of macroscopic crystals Fig. 4, bottom). Some advantages of AFM over TEM include its non-destructive nature, ease of sample preparation, and the ability to monitor guest–crystal interactions *in situ*.[32,83] We have also recently employed tuneable resistive pulse sensing (TRPS) for microcrystal batches to obtain size distributions and concentrations of microcrystal batches. This platform is increasingly used for quantifying extracellular vesicles and nanoparticles.[84]

3. Functionalization and applications

3.1. Enzyme scaffolds

It has been hypothesized that many enzymes and enzyme complexes have naturally evolved their scaffolding and active sites to reduce the distance that substrates need to diffuse

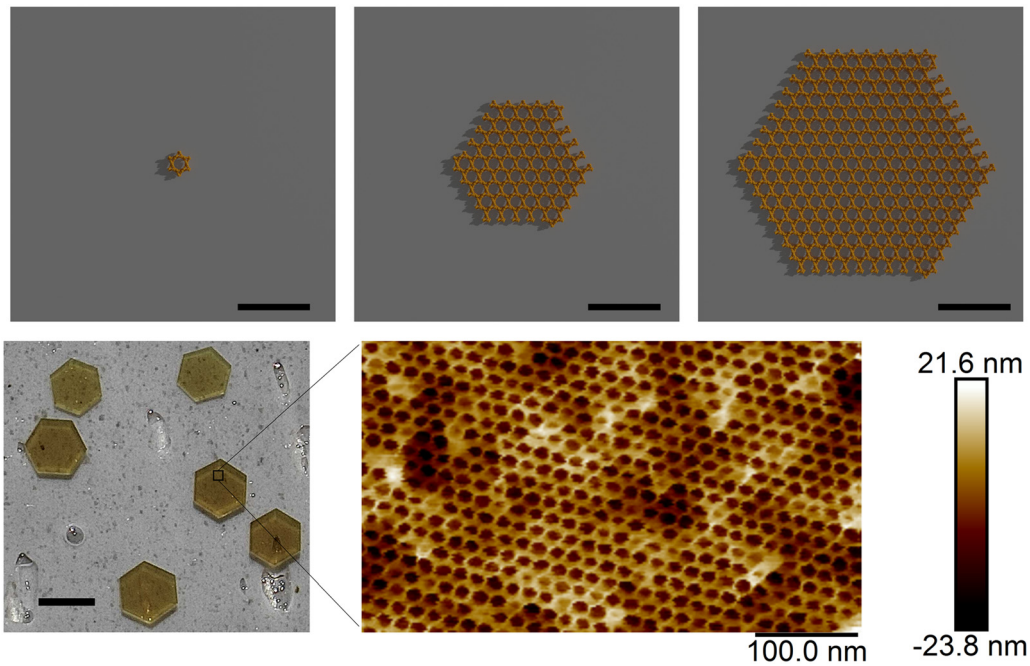

Fig. 4 Top: "CJ," an engineered variant of a putative polyisoprenoid binding protein (cj0420) from Campylobacter jejuni, easily crystallizes to form large, P622 crystals with characteristically large solvent channels. Hypothetical minimal nano-crystal assemblies are shown to illustrate that nanopore diameter is invariant with respect to crystal size. Scale bar = 100 nm. Bottom: Surfaces of porous CJ crystals can be validated by atomic force microscopy (AFM). The experimentally observed pore diameter is ~10-14 nm, while the distance between neighbouring pore centres is ~17-18 nm (as measured in ImageJ) (Scale bar = 0.5 mm (left), 100.0 nm (right)).

through a pathway from one enzyme's active site to another – putative examples from nature include a host of dehydrogenases[85–87] as well as more extreme examples like tryptophan synthase.[88–90] It has been previously argued that for efficient channelling to occur, the processing rate (that is, the rate at which the enzyme processes a given substrate within a confined geometry, defined as $k_{cat}N/V$, where k_{cat} is the catalytic constant of an enzyme, and N is the number of enzyme molecules confined to a given volume, V) must exceed the escape rate (*i.e.*, the frequency at which a substrate diffuses away from the confined enzyme, or D/r^2) for a particular enzyme; this is ultimately influenced by the catalytic efficiency of the enzyme, as well as the degree of confinement.[91,92] The controlled confinement within crystal pores offers a unique platform for enzyme immobilization and biocatalysis. By harnessing the ordered structure and tailored pore sizes of LPCs, enzymes can be selectively encapsulated, resulting in enhanced stability and catalytic efficiency.[93,94] The integration of enzymes within LPCs not only expands the scope of biocatalytic processes but also may enable sustainable industrial applications due to increased reusability.

Kowalski *et al.* from our group previously characterized enzymatic activity in CJ crystals.[47] CJ crystallizes to form *P*622 crystals with large pores (~13 nm) along their hexagonal face, along with smaller flanking pores (~3 nm). Because CJ crystals typically have a hexahistidine tag at the C-terminus, the resulting tags project into the major pore. As a result, guest proteins which also have a polyhistidine tag are able to interact with the histidine tag inside of the crystal *via* shared metal affinity,[95] resulting in non-covalent "tethering" of the protein guest. In this study, CJ crystals were grown to large sizes (>0.1 mm) using sitting-drop vapor diffusion, and subsequently cross-linked using glyoxal. The resulting scaffolds remained resistant to dissolution after transferring outside their mother liquor. After cross-linking, the crystals were soaked in a basic buffer containing nickel, in order to saturate the histidine tags in the crystal with nickel ions. Separately, bovine serum albumin (BSA), horseradish peroxidase (HRP), and glucose oxidase (GOX) were fluorescently labelled. Uptake of HRP was observed *via* confocal fluorescence microscopy, and crystal saturation was achieved after 16 hours. Co-loading of both GOX and HRP within the same crystal resulted in visible HRP activity throughout the crystal over a 2-minute period, after adding glucose and a fluorescent substrate. It was additionally observed that the crystal could be reused up to at least 5 recycles. These results demonstrated the feasibility of using protein crystals as a multi-enzyme scaffold, although this approach remained limited insofar as guest loading was non-covalent, and pH and metal dependent as a result of histidine tag tethering.

Recyclability of the scaffold in an industrial context is additionally a vital consideration. Heater *et al.* from the Chan group previously characterized the use of Cry3Aa crystals as a catalytic scaffold for the production of biodiesel from waste cooking oil.[96] Following their investigations of Cry3Aa structures, which revealed the presence of large pores (~50 Å × 50 Å), Heater *et al.* managed to confer lipase activity on crystals comprised of Cry3Aa-lipase fusion protein; the resulting crystals contained a lipase enzyme fused to the C-terminus of

Cry3Aa, projecting into the pore space of conventional Cry3Aa crystals.[96] The Cry3Aa-lipase fusion was subsequently screened (while the crystals were still encapsulated within cells) for improved activity *via* directed evolution. Optimized crystals displayed slightly higher K_m values, and greatly reduced k_{cat} values. When the crystals were purified *in vitro*, they demonstrated fatty acid transesterification to fatty acid methyl esters (FAME) in a variety of harsh solvent conditions and following prolonged exposure to increased temperatures. The same crystals were capable of an impressive 15 reuse cycles despite having been centrifuged, washed twice with hexane, and vacuum-dried between each cycle, with relative percent conversion remaining greater than 77%. The greatly reduced turnover may be explained as a result of suboptimal orientation of the immobilized enzyme. Similarly reduced catalytic efficiency was observed by Kowalski *et al.* for HRP immobilized within CJ crystal pores. It is probable that turnover and substrate binding are heavily influenced by a variety of factors that are difficult to control, such as the orientation of the enzyme active site relative to the crystal pore, as well as possible off-target binding between the guest enzyme and the pore wall.

An additional factor to consider with any reusable scaffold is modularity. It is self-evident that modification of a single platform to be able to accommodate multiple alternative guests is economically advantageous. Covalent installation of guest enzymes within a LPC is likewise desirable, as the resulting irreversible bond is neither pH or redox dependent, allowing the scaffold to tolerate a wider range of chemistries and solution conditions.[97] Following on their work with Cry3Aa-lipase crystals, Sun *et al.* attempted to introduce greater modularity in the Cry3Aa scaffold by fusing SpyCatcher at the C-terminus.[98] "SpyCatcher" is a 12.3 kDa protein, redesigned

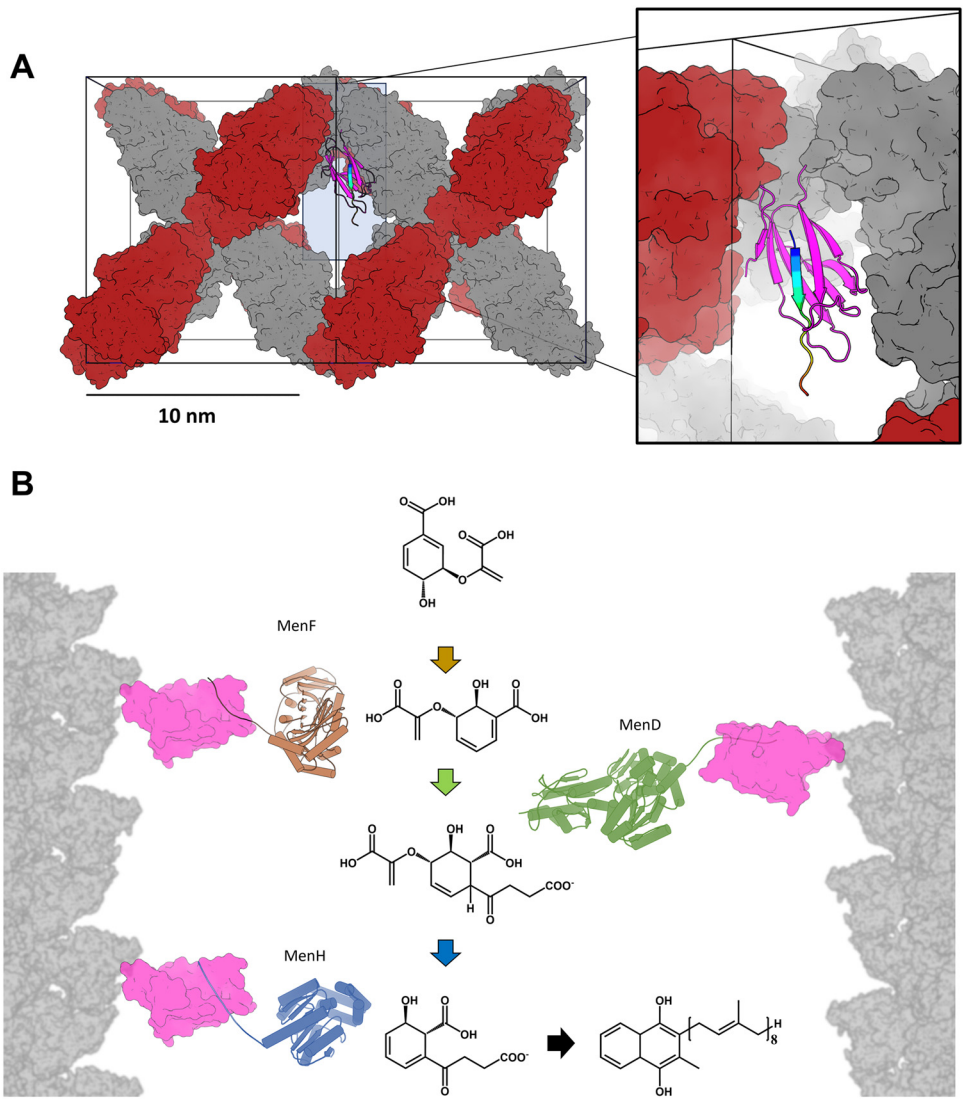

Fig. 5 (A) Cry3Aa crystals possess solvent channels formed between adjacent unit cells; the resulting crystal pore is large enough to accommodate guest enzymes displaying SpyTag (rainbow), covalently captured via a SpyCatcher domain (magenta) fused to the C-terminus of Cry3Aa (red). (B) Synthesis of menaquinol from chorismate is accomplished by the action of multiple enzymes (MenF, MenD, and MenH) in tandem, confined within the crystal pores (not to scale).

from the immunoglobulin-like CnaB2 domain from *Streptococcus pyogenes*, which is capable of reacting with a 13 amino acid peptide ("SpyTag") to form an intermolecular, isopeptide amide bond;[99] second and third generation variants which exhibit improved second-order rate constants have since been developed *via* directed evolution and rational design.[100] This platform has been used in a wide variety of applications, including enzyme immobilization,[101–103] recombinant protein purification,[104] and cyclization of protein termini to improve their stability.[105,106] After growing microcrystals from the fusion protein, guest loading was accomplished by sequentially soaking in three guest SpyTag002 fusion enzymes involved in the menaquinone synthesis pathway (MenF, MenD, and MenH) (Fig. 5), with the lowest molecular weight guests soaked into the crystal last.[98] Relative activity of the guest enzymes within the crystals was retained at higher temperatures, contrasting with the enzymes in free solution.[98] By introducing SpyCatcher at the Cry3Aa terminus within the crystals, the Cry3Aa scaffolds were able to accommodate multiple different guest enzymes in a modular fashion, thereby enabling the confinement of an entire metabolic pathway inside a single crystal scaffold.[98] The main limitation of this system is the narrowness of the crystal pores necessitates sequential guest loading on the basis of molecular weight/size. Crystals with larger diameter pores could allow larger domain guests to load without steric occlusion of the solvent channels.

3.2. Therapeutic delivery

Previously well-characterized platforms for therapeutic delivery of DNA, RNA, proteins, and small molecules include gold nanoparticles,[107–109] mesoporous silica particles,[110–112] liposomes,[113,114] and polymer-based scaffolds such as chitosan[115] and agarose-based hydrogels.[116] While each of these platforms are traditionally treated as independent frontiers in medical research, and the methods of synthesis can vary substantially, there is a considerable degree of overlap in terms of their experimental and analytical methods. Alongside these existing platforms, LPCs represent an emerging frontier.

Porous micro- and nanocrystals are particularly amenable to delivery applications, as larger protein crystals localized to the bloodstream could result in capillary occlusion.[117] Additionally, morphology and aspect ratio of particles, which can be difficult to control for certain protein crystals, has been shown to greatly influence circulation time and organ and tissue localization.[118] As a result, there have been few reported accounts testing delivery *in vivo* using LPCs. The Chan lab tested *in vivo* delivery of antimicrobial peptides housed in 1 μm-diameter Cry3Aa crystals in BALB/c mice *via* intravenous injection, and observed consistent localization of Cry3Aa crystals to the liver, lungs, and kidneys, up to 24 hours post-injection.[10] A more recent study by Yang *et al.* from the same group demonstrated delivery of p53 protein to mammalian cells *in vitro* using a modified version of Cry3Aa (dubbed Pos3Aa), which contained multiple lysine substitutions to increase the surface charge of the crystals. The Cry protein used to grow these crystals was fused to either mCherry fluorescent protein, or the p53 tumour-suppressing protein.[119] An additional justification for these mutations was based on ample evidence that uptake and endosomal escape are heavily dependent on the presence of numerous positively charged residues, such as lysine and arginine.[120–125] Independent staining of endosomes and crystals revealed that while cellular uptake occurred for both versions of Cry3Aa, endosomal escape into the cytoplasm was only observed for Pos3Aa crystals. Using different endocytic inhibitors, it was further observed that uptake was not receptor mediated, but instead occurred *via* macropinocytosis.[119] Crystals comprised of Pos3Aa-p53 fusion protein were able to sensitize mice to chemotherapy treatments, consistent with release and activity of p53 within the tumour cells. Cells exposed to crystals containing the mCherry fusion displayed diffuse fluorescence throughout the cytoplasm, which the authors had initially hypothesized may be due to dissolution of the crystals. Unexpectedly however, when they attempted to dissolve the crystals in PBS at physiological temperature and pH, they observed an independent band corresponding to the molecular weight of mCherry alone, rather than the fusion protein, thereby suggesting cleavage and release of the guest fusion protein; subsequent experiments indicated that sustained release of mCherry was observed over a period of three days.[119] Although the authors did not speculate as to the precise mechanism of cleavage, the results of this study demonstrate that LPCs can be engineered towards stable delivery of exogenous therapeutic proteins.

Outstanding questions related to the use of new LPCs in living systems include their potential cytotoxicity, immunogenicity, and their compatibility in vasculature, as previously mentioned. The question of cytotoxicity arises from both the potential toxicity of the scaffold protein, as well as the use of any reactive cross-linkers for stabilizing the crystals following synthesis. While our group has previously shown that large crystals grown from CJ do not induce significant cytotoxicity,[56] and Cry protein crystals do not appear to be cytotoxic or haemolytic,[10] parasporins (also derived from *Bacillus thuringiensis*) display clear cytotoxicity against HeLa and HT-29 cancer cells.[126] This example emphasizes the importance of careful evaluation of the potential *in vivo* effect of each scaffold protein, as well as consideration of possible carryover of undesirable bioactive substances (*e.g.* endotoxins) from the host organism used to grow the crystals. The second question as to what extent protein crystals can negatively impact circulation is implicitly addressed in the Chan group studies; intravenous injection of mice with $\sim$1 μm diameter crystals did not result in any apparent ill-effects on the mice.[10,119] In addition to safety, additional work remains related to specific cell targeting and tissue localization. In most of the described platforms, the crystals have remained largely unmodified, although it is conceivable that the protein sequence could be modified to display specific cell-binding motifs. Previous work with liposomes, dendrimers, and protein nanoparticles has demonstrated that binding and uptake by specific cell types can be achieved *via* decoration of the particle surface with nanobodies which recognize an epitope unique to a particular cell surface;[127] it is reasonable to believe that a similar strategy could be employed for targeting protein microcrystals.

In addition to delivery of antimicrobials and therapeutic proteins, cross-linked LPC microcrystals have also been explored as delivery vehicles for antigens. Previous work by St. Clair *et al.* compared the antigen response in rats between soluble human serum albumin (HSA), and glutaraldehyde-cross-linked HSA microcrystals (1–5 μm in diameter), and observed up to 30-fold increase in antibody titres for lightly-cross-linked HSA crystals.[128] Similar strategies have more recently shifted towards the use of protein nanoparticles[3,129] or peptide-based assemblies,[130] due to their relative ease of synthesis.

3.3. Templated fabrication of nanostructures

LPCs can also serve as a valuable template for the fabrication of inorganic nanoparticles, nanorods, dendrimers, and nanowires. Such nanostructures have a potentially broad range of applications, particularly in biosensing,[131–135] MRI contrast agents,[136] and targeted therapeutic delivery systems.[137,138] Traditional methods for synthesizing nanoparticles, nanorods, and nanowires occurs in bulk solution, where it can be difficult to control the size, shape, and stoichiometry of the produced structures. Through biomimetic mineralization, the ordered pore structure of the crystal provides a scaffold for the controlled nucleation and growth of inorganic materials. Depending on the side chains lining the crystal pores, concentration of metal ions can occur within the pore space or along the walls of the pores, supporting subsequent nucleation. For instance, nucleation and growth of magnetite nanoparticles within bacterial magnetosomes is believed to be dependent on the presence of multiple acidic residues in magnetosome-associating proteins.[139] Magnetite nucleation is achieved through a combination of iron binding within a confined region, and localized iron supersaturation.[140] Following nucleation within the crystal pores, metastable growth of larger nanoparticles and nanorods can be initiated by adjusting metal ion concentration, pH, or other solution conditions. Templating enables control over the size and composition of the resulting nanoparticles and facilitates the development of functional nanomaterials, in particular nanoparticles, nanorods, and nanowires. Within our own group, Kowalski *et al.* demonstrated sequestration of gold nanoparticles to the interior of CJ crystals[141] and subsequent nanorod growth (not published).

Previous methods involving the use of nanoporous protein scaffolds as templates for nanorod and nanoparticle production have relied on a diverse range of protein-based scaffolds, including hen egg white lysozyme (HEWL) crystals,[140,142,143] bacterial polyisoprenoid-binding proteins,[141] modified ferritin cages,[144,145] S-layer protein arrays[146] and BSA adsorbed to titanium oxide.[147] Ferritin cages, in particular, continue to be heavily investigated due to well-established protocols for heterologous expression, purification, and *in vitro* assembly.[148–152] While unmodified ferritin cages do not contain open-ended pores, they do possess an interior cavity on a comparable size scale to the porous systems described in this article (between 7 and 8 nm in diameter). While ferritin cages have been investigated in the context of delivery,[153–155] they have also been used to generate CdS,[156,157] ZnSe,[158] Pd,[159] and magnetite[160] nanoparticles of well-defined shapes and sizes, for potential use as MRI contrast agents or therapeutic delivery vectors.

Two-dimensional, porous arrangements of S-layer proteins, which are canonically involved in maintaining cell wall integrity in bacteria and archaea,[161] have received particularly strong focus in recent decades, following on the early work of Sleytr *et al.*[162] While S-layer proteins have been shown to self-assemble,[163,164] a more commonly reported method of synthesis involves cell lysis and isolation of cell wall components *via* ultracentrifugation.[164] Cytosolic expression and assembly of prokaryotic S-layer protein – GFP fusion protein has been achieved in yeast;[165] instead of forming sheets, the resulting crystals were rod-like (consistent with prior observations of *in vitro* self-assembly S-layer crystals),[166,167] although the porosity of the material was nevertheless confirmed by TEM. S-layer platforms have been used for deposition and nucleation of FePt nanoparticles from the gas phase,[168] as well as for controlled placement of ferromagnetic nanoparticles from solution.[169] In addition to nanoparticles, metal nanorods and nanowires[170,171] have also been constructed using similar strategies, typically in combination with chemical vapor deposition.

Similar templating strategies have also been used for generating biologically-derived nanostructures. A recent approach by Abe *et al.* from the Ueno group involves the use of protein nanotubes formed from *Trypanosoma brucei* cysteine protease cathepsin B (TbCatB), a protein which has been shown to crystallize *in vivo* in insect cells which have been baculovirus-infected.[172] The described approach displays many similarities with their previous work on RuBisCO nanotubes from *T. kodakaraensis*,[33] insofar as it utilizes a tubular protein assembly with a single channel, rather than a larger crystal containing a large number of pores. One-dimensional assembly ensures a confined space for templating of thin cylindrical materials, such as nanorods, nanowires, or filaments. In this particular context, the authors used the resulting tubular structures (which resist dissolving above pH 4) to generate proteinaceous filaments, stabilized by disulfide bonds between neighbouring cysteine residues.[172] This strategy could be extended towards the synthesis of proteinaceous nanorods and nanoparticles, towards potential applications in therapeutic delivery and catalysis.

3.4. Structure determination

Beyond the functional applications discussed above, LPCs have been explored as scaffolds for third-party proteins or other biomolecules which may otherwise be difficult or impossible to crystallize. Traditional X-ray diffraction methods are dependent on the molecular uniformity of the target within a crystal, yet certain molecules remain difficult to crystallize due to difficulties with expression in prokaryotic hosts, their susceptibility to detergents,[173] and for proteins with hydrophobic patches, there is the additional concern of poor protein solubility during crystallization screens.[174]

Because of these technical challenges, scaffold-assisted structure determination (SASD) has emerged as a potential strategy for generating a three-dimensional lattice for arbitrary proteins or biomolecules, by installing the target molecule upon a pre-existing crystal scaffold. Sufficiently high occupancy of the guest molecule throughout the crystal scaffold may result in resolvability of the guest, assuming a uniform orientation

and structure of the guest molecule across every unit cell of the scaffold. This approach was initially proposed by Nadrian Seeman in the 1980s as a DNA-based scaffold which could accommodate guest proteins.[175] Huber *et al.* from our group recently described a similar approach for resolving a small-molecule guest within a protein crystal. The scaffold protein was mutated to include a pore-facing cysteine, which was then conjugated to a small molecule guest.[11] Similar guest structure determination strategies have been recently reviewed.[176]

A recent platform in the spirit of this approach was recently reported by Orun *et al.* from our group in 2023.[177] In this platform, the porous crystal is a hybrid material consisting of replication factor E54 (RepE54)[178] and its 21-bp cognate DNA sequence, and contains protein complexes at the cell vertices. The resulting crystal scaffold was dubbed co-crystal 1 (CC1) (Fig. 6). Expansion of CC1 crystals from a single unit cell proceeds in a ''Lincoln log'' fashion, wherein two distinct protein–protein interfaces stabilize the crystal along the *z*-axis, while the crystal is further expanded in the *xy*-plane *via* the lengths of DNA running between the vertices; the resulting scaffolds were stabilized by chemical ligation of the 5′ and 3′ termini of the aligned DNA segments.[177] Critically, this topology theoretically allows the modular insertion of nearly any DNA sequence to support subsequent guest capture.

It should be noted that there are two potential limitations with this type of hybrid scaffold. The first is the observed tendency of the crystals to adopt an interpenetrating lattice which results in a steep reduction in overall porosity, restricting the number of possible guest molecules. The second limitation is a consequence of using DNA as a co-crystallizing element. To stabilize the co-crystals outside of their mother liquor, it is necessary to ligate the termini of DNA oligomers between the neighbouring unit cells; because of this, the 5′ and 3′ ends of the DNA molecules must be properly aligned. Due to the biophysical constraints of a stable right-handed DNA helix, this means that the length of DNA between the stacked protein vertices must be a multiple of around 10–11 base pairs. Successfully growing well-diffracting crystal scaffolds becomes more challenging as greater flexibility in the scaffold is introduced, which can limit diffraction resolution for large DNA expansion co-crystals. Notably, protein–DNA co-crystals have many other potential applications beyond structure determination; for instance, an increase in flexibility and pore size, combined with their inherent biocompatibility, may be useful for a wide range of biomedical and biomaterials applications such as hybrid biomaterials, biosensing, and therapeutic delivery.[179–184]

3.5. Emerging and future applications

In addition to the aforementioned applications, LPC scaffolds have been utilized for a variety of niche applications, the majority of which are dependent on the unique properties of the protein itself. For instance, the CJ crystals that our lab routinely works with are able to rapidly adsorb nucleic acids to their interior,[32,185] and this property is currently being exploited by our group across multiple projects.

There is a precedent for the use of recombinant proteins in textile applications. Spider silk,[186,187] elastin,[188] resilin,[189,190] collagen,[191] fibroin,[192] and keratin[193] are all well-characterized structural proteins, and have been utilized in textiles in recent years, most commonly *via* electrospinning of individual fibres, or casting and self-assembly in foams and hydrogels. However, precisely controlled porosity is difficult in such systems. In pursuit of multifunctional textiles involving attachment of protein crystal depots, Hartje *et al.* from our group recently demonstrated integration of individual lysozyme and CJ crystals on bulk cotton, *via* chemical cross-linking with dihydrazides or dialdehydes, respectively.[194] The resulting crystals were able to adsorb guest sulforhodamine-labeled cytochrome P450 protein, although the activity of guest P450 enzyme was not tested. Despite repeated laundering of the functionalized fabrics, at least 20% of the attached crystals were retained when chemically cross-linked to fabric.[194] The authors suggest that

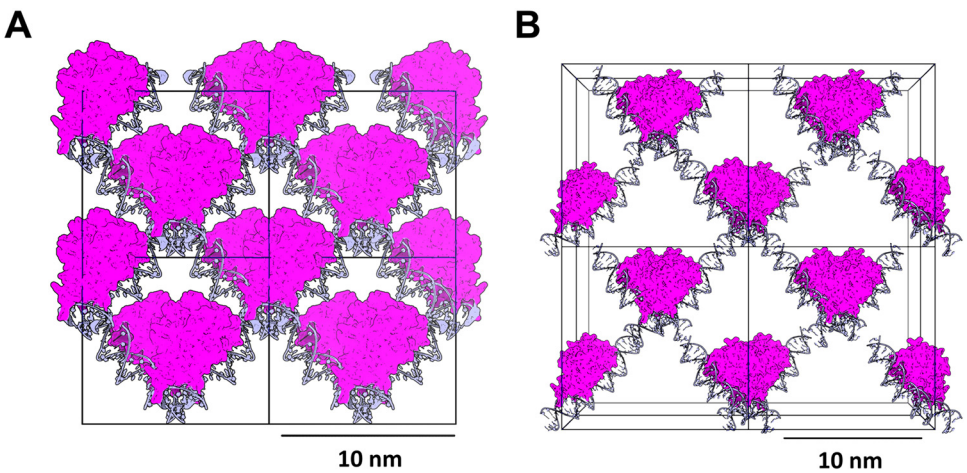

Fig. 6 (A) Isoreticular co-crystals (ICCs) consist predominantly of stacked DNA (light blue) connected via an orthogonal stack of RepE54 protein (magenta). (B) The co-crystal pores can be expanded while maintaining the same topology via introduction of additional bases in the DNA sequences. To ensure that the ends of the DNA molecules are correctly oriented for ligation, the length of the DNA is limited to multiples of 10-11 base pairs. Scale bar = 100.0 Å = 10 nm.

crystal retention might be improved *via* more robust chemical crosslinking;[194] additional strategies could involve *in situ* crystal growth on the surface of the fabric, which could reduce downstream handling and transfer of crystals. This approach may enable additional functionalization of cloth surfaces, particularly when combined with biosensing crystals or scaffolds which interact with specific pathogens.

Yet another novel application of LPCs is as a marker for mark-release-recapture (MRR) studies. It was previously demonstrated that CJ crystals were able to adsorb DNA to the crystal interior,[185] so Stuart *et al.* from our group synthesized CJ microcrystals loaded with a synthetic DNA marker; after saturating these microcrystals with DNA, they were deposited in tubs of stagnant water and allowed to incubate for several days alongside mosquito larvae.[185] Emerging adult mosquitoes were subsequently captured and reared in an insectary, whereupon they were sacrificed, and the original barcode sequence was recovered from the adult mosquitoes *via* qPCR-based detection and next-generation sequencing.[185] This study demonstrates a novel application of LPCs for marking and detection of mosquitoes, which have traditionally relied on fluorescent powders,[195] paints/dyes, or radioisotopes.[196]

4. Conclusions

This review has described both the synthesis and applications of several existing LPC platforms, although these represent a small fraction of the opportunities for this material family. Due to the inherent structural and functional diversity of proteins, the number of possible lattice structures and functionality is limited only by human imagination. The past year alone has seen extremely rapid advances in machine learning-based methods,[197–199] and it is increasingly possible to identify sequences that conform to any desired tertiary structure. In 2023, the Baker group reported designed 3D protein crystals capable of rapid *in vitro* self-assembly.[200] Additional machine learning tools, such as AlphaFold, have been used to predict allosteric and protein–ligand interactions,[201] and may be used to alter the structure and binding affinities of LPCs. With the advent of reliable protein crystal design, we anticipate rapid growth in the number of engineered crystals with functional applications. This emerging family of high-precision biomaterials represents a novel frontier for catalysis, therapeutic delivery, and a host of unexplored applications.

Author contributions

The manuscript was written by A. A. J., and edited by C. D. S.

Conflicts of interest

There are no conflicts to declare.

Acknowledgements

A. A. J. was supported during this work with Anschutz Family Foundation funding. Figures were prepared in PyMOL 2.3.1, ChemDraw Professional 22.2.0.3300, and Blender 4.0.

Notes and references

1 M. B. Stie, K. Kalouta, V. Vetri and V. Foderà, *J. Controlled Release*, 2022, **344**, 12–25.
2 N. C. Abascal and L. Regan, *Open Biol.*, 2018, **8**, 180113.
3 B. Zhang, C. W. Chao, Y. Tsybovsky, O. M. Abiona, G. B. Hutchinson, J. I. Moliva, A. S. Olia, A. Pegu, E. Phung, G. B. E. Stewart-Jones, R. Verardi, L. Wang, S. Wang, A. Werner, E. S. Yang, C. Yap, T. Zhou, J. R. Mascola, N. J. Sullivan, B. S. Graham, K. S. Corbett and P. D. Kwong, *Sci. Rep.*, 2020, **10**, 18149.
4 X. Tan, H. Chen, C. Gu, J. Zang, T. Zhang, H. Wang and G. Zhao, *Commun. Chem.*, 2020, **3**, 151.
5 E. Sasaki, D. Böhringer, M. van de Waterbeemd, M. Leibundgut, R. Zschoche, A. J. R. Heck, N. Ban and D. Hilvert, *Nat. Commun.*, 2017, **8**, 14663.
6 C. Huerta-López and J. Alegre-Cebollada, *Nanomaterials*, 2021, **11**(7), 1656.
7 M. Charrier, D. Li, V. R. Mann, L. Yun, S. Jani, B. Rad, B. E. Cohen, P. D. Ashby, K. R. Ryan and C. M. Ajo-Franklin, *ACS Synth. Biol.*, 2019, **8**, 181–190.
8 Y.-M. Tu, W. Song, T. Ren, Y. Shen, R. Chowdhury, P. Rajapaksha, T. E. Culp, L. Samineni, C. Lang, A. Thokkadam, D. Carson, Y. Dai, A. Mukthar, M. Zhang, A. Parshin, J. N. Sloand, S. H. Medina, M. Grzelakowski, D. Bhattacharya, W. A. Phillip, E. D. Gomez, R. J. Hickey, Y. Wei and M. Kumar, *Nat. Mater.*, 2020, **19**, 347–354.
9 T. R. Huber, L. F. Hartje, E. C. McPherson, A. E. Kowalski and C. D. Snow, *Small*, 2017, **13**, 1602703.
10 Z. Yang, J. Zheng, C.-F. Chan, I. L. K. Wong, B. S. Heater, L. M. C. Chow, M. M. M. Lee and M. K. Chan, *Biomaterials*, 2019, **217**, 119286.
11 T. R. Huber, E. C. McPherson, C. E. Keating and C. D. Snow, *Bioconjugate Chem.*, 2018, **29**, 17–22.
12 A. Tiessen, P. Pérez-Rodríguez and L. J. Delaye-Arredondo, *BMC Res. Notes*, 2012, **5**, 85.
13 P. L. Privalov, in *Advances in Protein Chemistry*, ed. C. B. Anfinsen, J. T. Edsall and F. M. Richards, Academic Press, 1979, vol. 33, pp. 167–241.
14 Y. Sawada and S. Honda, *Biophys. J.*, 2006, **91**, 1213–1223.
15 S. Nepomnyachiy, N. Ben-Tal and R. Kolodny, *Proc. Natl. Acad. Sci. U. S. A.*, 2017, **114**, 11703–11708.
16 O. Svensson, M. Gilski, D. Nurizzo and M. W. Bowler, *IUCrJ*, 2019, **6**, 822–831.
17 L. Xu, S. D. Benson and R. M. Burnett, *J. Struct. Biol.*, 2007, **157**, 424–431.
18 K. O. Ramberg, S. Engilberge, T. Skorek and P. B. Crowley, *J. Am. Chem. Soc.*, 2021, **143**, 1896–1907.
19 Y.-T. Lai, E. Reading, G. L. Hura, K.-L. Tsai, A. Laganowsky, F. J. Asturias, J. A. Tainer, C. V. Robinson and T. O. Yeates, *Nat. Chem.*, 2014, **6**, 1065–1071.
20 J. Li, J. Carroll and D. J. Ellar, *Nature*, 1991, **353**, 815–821.
21 J. L. Miller, J. L. Coq, A. Hodes, R. Barbalat, J. F. Miller and P. Ghosh, *PLoS Biol.*, 2008, **6**, e131.
22 K. A. Kantardjieff and B. Rupp, *Protein Sci.*, 2003, **12**, 1865–1871.
23 C. X. Weichenberger and B. Rupp, *Acta Crystallogr., Sect. D: Biol. Crystallogr.*, 2014, **70**, 1579–1588.
24 C. M. C. Lobley, J. Sandy, J. Sanchez-Weatherby, M. Mazzorana, T. Krojer, R. P. Nowak and T. L. Sorensen, *Acta Crystallogr., Sect. D: Biol. Crystallogr.*, 2016, **72**, 629–640.
25 J. Sanchez-Weatherby and I. Moraes, *Adv. Exp. Med. Biol.*, 2016, **922**, 73–89.
26 A. McPherson and J. A. Gavira, *Acta Crystallogr., Sect. F: Struct. Biol. Cryst. Commun.*, 2013, **70**, 2–20.
27 S. Abe, H. Tabe, H. Ijiri, K. Yamashita, K. Hirata, K. Atsumi, T. Shimoi, M. Akai, H. Mori, S. Kitagawa and T. Ueno, *ACS Nano*, 2017, **11**, 2410–2419.
28 T. Ueno, *Chem. - Eur. J.*, 2013, **19**, 9096–9102.

29 M. Kojima, S. Abe and T. Ueno, *Biomater. Sci.*, 2022, **10**, 354–367.
30 H. Tabe, H. Takahashi, T. Shimoi, S. Abe, T. Ueno and Y. Yamada, *Appl. Catal., B*, 2018, **237**, 1124–1129.
31 J. M. Thomas, *Nature*, 2012, **491**, 186–187.
32 D. Wang, J. D. Stuart, A. A. Jones, C. D. Snow and M. J. Kipper, *Nanoscale*, 2021, **13**, 10871–10881.
33 T. K. Nguyen, H. Negishi, S. Abe and T. Ueno, *Chem. Sci.*, 2019, **10**, 1046–1051.
34 I. Boyton, S. C. Goodchild, D. Diaz, A. Elbourne, L. E. Collins-Praino and A. Care, *ACS Omega*, 2022, **7**, 823–836.
35 S. L. Heinz-Kunert, A. Pandya, V. T. Dang, P. N. Tran, S. Ghosh, D. McElheny, B. D. Santarsiero, Z. Ren and A. I. Nguyen, *J. Am. Chem. Soc.*, 2022, **144**, 7001–7009.
36 J. Ke, J. Zhang, J. Li, J. Liu and S. Guan, *Int. J. Mol. Sci.*, 2022, **23**, 12071.
37 C. Wu and H. Wang, *ChemBioChem*, 2023, **24**, e202300018.
38 R. Moral and S. Paul, *Langmuir*, 2024, **40**, 882–895.
39 A. Méndez-Ardoy, I. Insua, J. R. Granja and J. Montenegro, *Methods Mol. Biol.*, 2022, **2371**, 449–466.
40 D. J. Rubin, S. Amini, F. Zhou, H. Su, A. Miserez and N. S. Joshi, *ACS Nano*, 2015, **9**, 3360–3368.
41 F. Castro, A. Ferreira, J. A. Teixeira and F. Rocha, *Cryst. Growth Des.*, 2016, **16**, 3748–3755.
42 F. Castro, I. Cunha, A. Ferreira, J. A. Teixeira and F. Rocha, *Chem. Eng. Res. Des.*, 2022, **178**, 575–582.
43 H. Mori, R. Ito, H. Nakazawa, M. Sumida, F. Matsubara and Y. Minobe, *J. Gen. Virol.*, 1993, **74**, 99–102.
44 M. S. Nair, M. M. Lee, A. Bonnegarde-Bernard, J. A. Wallace, D. H. Dean, M. C. Ostrowski, R. W. Burry, P. N. Boyaka and M. K. Chan, *PLoS One*, 2015, **10**, e0127669.
45 S. Abe, J. Tanaka, M. Kojima, S. Kanamaru, K. Hirata, K. Yamashita, A. Kobayashi and T. Ueno, *Sci. Rep.*, 2022, **12**, 16031.
46 J. C. Falkner, A. M. Al-Somali, J. A. Jamison, J. Zhang, S. L. Adrianse, R. L. Simpson, M. K. Calabretta, W. Radding, G. N. Phillips and V. L. Colvin, *Chem. Mater.*, 2005, **17**, 2679–2686.
47 A. E. Kowalski, L. B. Johnson, H. K. Dierl, S. Park, T. R. Huber and C. D. Snow, *Biomater. Sci.*, 2019, **7**, 1898–1904.
48 K. Han, Z. Zhang and F. A. Tezcan, *J. Am. Chem. Soc.*, 2023, **145**, 19932–19944.
49 R. Adalat, F. Saleem, N. Crickmore, S. Naz and A. R. Shakoori, *Toxins*, 2017, **9**, 80.
50 J. Herrmann, F. Jabbarpour, P. G. Bargar, J. F. Nomellini, P.-N. Li, T. J. Lane, T. M. Weiss, J. Smit, L. Shapiro and S. Wakatsuki, *Biophys. J.*, 2017, **112**, 1841–1851.
51 C. J. Comerci, J. Herrmann, J. Yoon, F. Jabbarpour, X. Zhou, J. F. Nomellini, J. Smit, L. Shapiro, S. Wakatsuki and W. E. Moerner, *Nat. Commun.*, 2019, **10**, 2731.
52 V. R. Mann, F. Manea, N. J. Borys, C. M. Ajo-Franklin and B. E. Cohen, *Biochemistry*, 2021, **60**, 1063–1074.
53 K. Lu, W. Ye, L. Zhou, L. B. Collins, X. Chen, A. Gold, L. M. Ball and J. A. Swenberg, *J. Am. Chem. Soc.*, 2010, **132**, 3388–3399.
54 E.-K. Yan, H.-L. Cao, C.-Y. Zhang, Q.-Q. Lu, Y.-J. Ye, J. He, L.-J. Huang and D.-C. Yin, *RSC Adv.*, 2015, **5**, 26163–26174.
55 F. A. Quiocho and F. M. Richards, *Proc. Natl. Acad. Sci. U. S. A.*, 1964, **52**, 833–839.
56 L. F. Hartje, H. T. Bui, D. A. Andales, S. P. James, T. R. Huber and C. D. Snow, *ACS Biomater. Sci. Eng.*, 2018, **4**, 826–831.
57 A. R. Orun, S. Dmytriw, A. Vajapayajula and C. D. Snow, *Crystals*, 2022, **12**, 49.
58 Q. Zhang, E. Crosland and D. Fabris, *Anal. Chim. Acta*, 2008, **627**, 117–128.
59 C. J. Lusty, *J. Appl. Cryst.*, 1999, **32**, 106–112.
60 T. Hiromoto, T. Ikura, E. Honjo, M. Blaber, R. Kuroki and T. Tamada, *Front. Mol. Biosci.*, 2022, **9**, 908394.
61 M. Pu, Z. Xu, Y. Peng, Y. Hou, D. Liu, Y. Wang, H. Liu, G. Song and Z.-J. Liu, *Protein Cell*, 2018, **9**, 659–663.
62 D.-A. Silva, L. Stewart, K.-H. Lam, R. Jin and D. Baker, *FEBS J.*, 2018, **285**, 1783–1785.
63 J. Fauser, S. Savitskiy, M. Fottner, V. Trauschke and B. Gulen, *Bioconjugate Chem.*, 2020, **31**, 1883–1892.
64 A. Susmitha, J. S. Arya, L. Sundar, K. K. Maiti and K. M. Nampoothiri, *J. Biotechnol.*, 2023, **367**, 11–19.
65 H. H. Wang, B. Altun, K. Nwe and A. Tsourkas, *Angew. Chem. Int. Ed.*, 2017, **56**, 5349–5352.
66 L.-X. Cai, Y.-Q. Lin, Y.-M. Chu, X.-P. Chen, L.-X. Liu, M. Zhang and G.-Y. Zhang, *Bio. Protoc.*, 2022, **12**, e4282.
67 C. Liu, J. Hua, P. F. Ng and B. Fei, *J. Mater. Sci. Technol.*, 2021, **63**, 182–191.
68 J. Lee, M. Ju, O. H. Cho, Y. Kim and K. T. Nam, *Adv. Sci.*, 2019, **6**, 1801255.
69 D. J. Raven, C. Earland and M. Little, *Biochim. Biophys. Acta, Protein Struct.*, 1971, **251**, 96–99.
70 F. Müller, A. Graziadei and J. Rappsilber, *Anal. Chem.*, 2019, **91**, 9041–9048.
71 K. Stahl, A. Graziadei, T. Dau, O. Brock and J. Rappsilber, *Nat. Biotechnol.*, 2023, 1–10.
72 U. Schweizer, T. Hey, G. Lipps and G. Krauss, *Nucleic Acids Res.*, 1999, **27**, 3183–3189.
73 S. Zhang, D. H. Adamson, R. K. Prud'homme and A. J. Link, *Polym. Chem.*, 2011, **2**, 665–671.
74 R. A. Luse and A. D. McLaren, *Photochem. Photobiol.*, 1963, **2**, 343–360.
75 W. Sutherland, *London, Edinburgh Dublin Philos. Mag. J. Sci.*, 1905, **9**(54), 781–785.
76 A. Einstein, *Ann. Phys.*, 1905, **17**, 549–560.
77 A. Sauter, F. Roosen-Runge, F. Zhang, G. Lotze, R. M. J. Jacobs and F. Schreiber, *J. Am. Chem. Soc.*, 2015, **137**, 1485–1491.
78 R. Maier, G. Zocher, A. Sauter, S. Da Vela, O. Matsarskaia, R. Schweins, M. Sztucki, F. Zhang, T. Stehle and F. Schreiber, *Cryst. Growth Des.*, 2020, **20**, 7951–7962.
79 W. Tian, W. Li and H. Yang, *Cryst. Growth Des.*, 2023, **23**, 5181–5193.
80 D. W. Oxtoby, *J. Phys.: Condens. Matter*, 1992, **4**, 7627.
81 R. Schubert, A. Meyer, K. Dierks, S. Kapis, R. Reimer, H. Einspahr, M. Perbandt and C. Betzel, *J. Appl. Cryst.*, 2015, **48**, 1476–1484.
82 Y. Zhou, Z. Dong, O. Terasaki and Y. Ma, *Acc. Mater. Res.*, 2022, **3**, 110–121.
83 D. Wang, M. Hedayati, J. D. Stuart, L. Y. C. Madruga, K. C. Popat, C. D. Snow and M. J. Kipper, *Mater. Today Nano*, 2023, **24**, 100432.
84 G. R. Willmott, *Anal. Chem.*, 2018, **90**, 2987–2995.
85 S. Kumar, S. Sega, J. K. Lynn-Barbe, D. L. Harris, J. T. Koehn, D. C. Crans and D. C. Crick, *Pathogens*, 2023, **12**, 1171.
86 J. Škerlová, J. Berndtsson, H. Nolte, M. Ott and P. Stenmark, *Nat. Commun.*, 2021, **12**, 5277.
87 Ž. M. Svedružić, I. Odorčić, C. H. Chang and D. Svedružić, *Sci. Rep.*, 2020, **10**, 10404.
88 P. Mehrabi, S. Sung, D. von Stetten, A. Prester, C. E. Hatton, S. Kleine-Döpke, A. Berkes, G. Gore, J.-P. Leimkohl, H. Schikora, M. Kollewe, H. Rohde, M. Wilmanns, F. Tellkamp and E. C. Schulz, *Nat. Commun.*, 2023, **14**(1), 2365.
89 M. F. Dunn, *Arch. Biochem. Biophys.*, 2012, **519**, 154–166.
90 M. F. Dunn, D. Niks, H. Ngo, T. R. M. Barends and I. Schlichting, *Trends Biochem. Sci.*, 2008, **33**, 254–264.
91 M. Castellana, M. Z. Wilson, Y. Xu, P. Joshi, I. M. Cristea, J. D. Rabinowitz, Z. Gitai and N. S. Wingreen, *Nat. Biotechnol.*, 2014, **32**, 1011–1018.
92 J. P. Dexter, P. S. Ward, T. Dasgupta, A. M. Hosios, J. Gunawardena and M. G. Vander Heiden, *J. Biol. Chem.*, 2018, **293**, 20051–20061.
93 K. Xu, X. Chen, R. Zheng and Y. Zheng, *Front. Bioeng. Biotechnol.*, 2020, **8**, 660.
94 T. K. Nguyen, S. Abe, M. Kasamatsu, B. Maity, K. Yamashita, K. Hirata, M. Kojima and T. Ueno, *ACS Appl. Nano Mater.*, 2021, **4**, 1672–1681.
95 R. D. Healey, L. Couillaud, F. Hoh, A. Mouhand, A. Fouillen, P. Couvineau, S. Granier and C. Leyrat, *Commun. Chem.*, 2023, **6**, 1–13.
96 B. S. Heater, W. S. Chan, M. M. Lee and M. K. Chan, *Biotechnol. Biofuels*, 2019, **12**, 165.
97 S. Gad and S. Ayakar, *Biotechnol. Rep.*, 2021, **32**, e00670.
98 Q. Sun, B. S. Heater, T. L. Li, W. Ye, Z. Guo and M. K. Chan, *Bioconjugate Chem.*, 2022, **33**, 386–396.
99 B. Zakeri, J. O. Fierer, E. Celik, E. C. Chittock, U. Schwarz-Linek, V. T. Moy and M. Howarth, *Proc. Natl. Acad. Sci. U. S. A.*, 2012, **109**, E690–E697.
100 A. H. Keeble, P. Turkki, S. Stokes, I. N. A. Khairil Anuar, R. Rahikainen, V. P. Hytönen and M. Howarth, *Proc. Natl. Acad. Sci. U. S. A.*, 2019, **116**, 26523–26533.
101 J. Tian, R. Jia, D. Wenge, H. Sun, Y. Wang, Y. Chang and H. Luo, *Biotechnol. Lett.*, 2021, **43**, 1075–1087.

102 G. P. Anderson, J. L. Liu, L. C. Shriver-Lake, D. Zabetakis, V. A. Sugiharto, H.-W. Chen, C.-R. Lee, G. N. Defang, S.-J. L. Wu, N. Venkateswaran and E. R. Goldman, *Anal. Chem.*, 2019, **91**, 9424–9429.
103 M. Liu, Y. Song, Y.-H. P. J. Zhang and C. You, *ChemSusChem*, 2023, **16**, e202202153.
104 I. N. A. Khairil Anuar, A. Banerjee, A. H. Keeble, A. Carella, G. I. Nikov and M. Howarth, *Nat. Commun.*, 2019, **10**, 1734.
105 C. Schoene, J. O. Fierer, S. P. Bennett and M. Howarth, *Angew. Chem. Int. Ed.*, 2014, **53**, 6101–6104.
106 S. Zhang, Q. Ren, S. J. Novick, T. S. Strutzenberg, P. R. Griffin and H. Bao, *Nat. Commun.*, 2021, **12**, 5451.
107 S. Guo, Y. Huang, Q. Jiang, Y. Sun, L. Deng, Z. Liang, Q. Du, J. Xing, Y. Zhao, P. C. Wang, A. Dong and X.-J. Liang, *ACS Nano*, 2010, **4**, 5505–5511.
108 J. Guo, M. J. Armstrong, C. M. O'Driscoll, J. D. Holmes and K. Rahme, *RSC Adv.*, 2015, **5**, 17862–17871.
109 T. Ruks, K. Loza, M. Heggen, C. Ottmann, P. Bayer, C. Beuck and M. Epple, *ChemBioChem*, 2021, **22**, 1456–1463.
110 C. Bharti, U. Nagaich, A. K. Pal and N. Gulati, *Int. J. Pharm. Investig.*, 2015, **5**, 124–133.
111 F. Rizzi, R. Castaldo, T. Latronico, P. Lasala, G. Gentile, M. Lavorgna, M. Striccoli, A. Agostiano, R. Comparelli, N. Depalo, M. L. Curri and E. Fanizza, *Molecules*, 2021, **26**(14), 4247.
112 M. Vallet-Regí, F. Schüth, D. Lozano, M. Colilla and M. Manzano, *Chem. Soc. Rev.*, 2022, **51**, 5365–5451.
113 H. Elsana, T. O. B. Olusanya, J. Carr-Wilkinson, S. Darby, A. Faheem and A. A. Elkordy, *Sci. Rep.*, 2019, **9**, 15120.
114 M. A. Obeid, A. Elburi, L. C. Young, A. B. Mullen, R. J. Tate and V. A. Ferro, *Mol. Pharmaceutics*, 2017, **14**, 2450–2458.
115 B. R. Lee, K. T. Oh, H. J. Baik, Y. S. Youn and E. S. Lee, *Int. J. Pharm.*, 2010, **392**, 78–82.
116 N. Ninan, A. Forget, V. P. Shastri, N. H. Voelcker and A. Blencowe, *ACS Appl. Mater. Interfaces*, 2016, **8**, 28511–28521.
117 M. Cooley, A. Sarode, M. Hoore, D. A. Fedosov, S. Mitragotri and A. S. Gupta, *Nanoscale*, 2018, **10**, 15350–15364.
118 P. Decuzzi, B. Godin, T. Tanaka, S. Y. Lee, C. Chiappini, X. Liu and M. Ferrari, *J. Controlled Release*, 2010, **141**, 320–327.
119 Z. Yang, M. M. M. Lee and M. K. Chan, *Biomaterials*, 2021, **271**, 120759.
120 I. Nakase, K. Noguchi, A. Aoki, T. Takatani-Nakase, I. Fujii and S. Futaki, *Sci. Rep.*, 2017, **7**, 1991.
121 S. Silva, A. J. Almeida and N. Vale, *Biomolecules*, 2019, **9**, 22.
122 I. M. S. Degors, C. Wang, Z. U. Rehman and I. S. Zuhorn, *Acc. Chem. Res.*, 2019, **52**, 1750–1760.
123 Z. Sun, J. Huang, Z. Fishelson, C. Wang and S. Zhang, *Biomedicines*, 2023, **11**, 1971.
124 B. R. McNaughton, J. J. Cronican, D. B. Thompson and D. R. Liu, *Proc. Natl. Acad. Sci. U. S. A.*, 2009, **106**, 6111–6116.
125 J. Yin, Q. Wang, S. Hou, L. Bao, W. Yao and X. Gao, *J. Am. Chem. Soc.*, 2018, **140**, 17234–17240.
126 M. A. M. Aboul-Soud, M. Z. Al-Amri, A. Kumar, Y. A. Al-Sheikh, A. E. Ashour and T. A. El-Kersh, *Molecules*, 2019, **24**, 506.
127 Y. Hu, C. Liu and S. Muyldermans, *Front. Immunol.*, 2017, **8**, 1442.
128 N. S. Clair, B. Shenoy, L. D. Jacob and A. L. Margolin, *Proc. Natl. Acad. Sci. U. S. A.*, 1999, **96**, 9469–9474.
129 T. K. Tan, P. Rijal, R. Rahikainen, A. H. Keeble, L. Schimanski, S. Hussain, R. Harvey, J. W. P. Hayes, J. C. Edwards, R. K. McLean, V. Martini, M. Pedrera, N. Thakur, C. Conceicao, I. Dietrich, H. Shelton, A. Ludi, G. Wilsden, C. Browning, A. K. Zagrajek, D. Bialy, S. Bhat, P. Stevenson-Leggett, P. Hollinghurst, M. Tully, K. Moffat, C. Chiu, R. Waters, A. Gray, M. Azhar, V. Mioulet, J. Newman, A. S. Asfor, A. Burman, S. Crossley, J. A. Hammond, E. Tchilian, B. Charleston, D. Bailey, T. J. Tuthill, S. P. Graham, H. M. E. Duyvesteyn, T. Malinauskas, J. Huo, J. A. Tree, K. R. Buttigieg, R. J. Owens, M. W. Carroll, R. S. Daniels, J. W. McCauley, D. I. Stuart, K.-Y. A. Huang, M. Howarth and A. R. Townsend, *Nat. Commun.*, 2021, **12**, 542.
130 R. F. Q. Grenfell, L. M. Shollenberger, E. F. Samli and D. A. Harn, *Clin. Vaccine Immunol.*, 2015, **22**, 336–343.
131 S. Malik, J. Singh, R. Goyat, Y. Saharan, V. Chaudhry, A. Umar, A. A. Ibrahim, S. Akbar, S. Ameen and S. Baskoutas, *Heliyon*, 2023, **9**, e19929.
132 X. Liu, Y. Qiu, D. Jiang, F. Li, Y. Gan, Y. Zhu, Y. Pan, H. Wan and P. Wang, *Microsyst. Nanoeng.*, 2022, **8**, 1–15.
133 C. Yu and J. Irudayaraj, *Anal. Chem.*, 2007, **79**, 572–579.
134 R. Elghanian, J. J. Storhoff, R. C. Mucic, R. L. Letsinger and C. A. Mirkin, *Science*, 1997, **277**, 1078–1081.
135 N. L. Rosi and C. A. Mirkin, *Chem. Rev.*, 2005, **105**, 1547–1562.
136 H. Wei, A. Wiśniowska, J. Fan, P. Harvey, Y. Li, V. Wu, E. C. Hansen, J. Zhang, M. G. Kaul, A. M. Frey, G. Adam, A. I. Frenkel, M. G. Bawendi and A. Jasanoff, *Proc. Natl. Acad. Sci. U. S. A.*, 2021, **118**, e2102340118.
137 J. M. Rae and B. Jachimska, *Nanoscale*, 2021, **13**, 2703–2713.
138 T. Niidome, A. Shiotani, T. Mori and Y. Katayama, *J. Controlled Release*, 2010, **148**, e65–6.
139 A. Yamagishi, K. Narumiya, M. Tanaka, T. Matsunaga and A. Arakaki, *Sci. Rep.*, 2016, **6**, 35670.
140 M. Savchenko, V. Sebastian, M. T. Lopez-Lopez, A. Rodriguez-Navarro, L. Alvarez De Cienfuegos, C. Jimenez-Lopez and J. A. Gavira, *Cryst. Growth Des.*, 2023, **23**, 4032–4040.
141 A. E. Kowalski, T. R. Huber, T. W. Ni, L. F. Hartje, K. L. Appel, J. W. Yost, C. J. Ackerson and C. D. Snow, *Nanoscale*, 2016, **8**, 12693–12696.
142 M. Guli, E. M. Lambert, M. Li and S. Mann, *Angew. Chem., Int. Ed.*, 2010, **49**, 520–523.
143 O. Deschaume, B. De Roo, M. J. Van Bael, J.-P. Locquet, C. Van Haesendonck and C. Bartic, *Chem. Mater.*, 2014, **26**, 5383–5393.
144 C. Lu, B. Maity, X. Peng, N. Ito, S. Abe, X. Sheng, T. Ueno and D. Lu, *Commun. Chem.*, 2022, **5**, 39.
145 B. Maity, Y. Hishikawa, D. Lu and T. Ueno, *Polyhedron*, 2019, **172**, 104–111.
146 S. S. Mark, M. Bergkvist, P. Bhatnagar, C. Welch, A. L. Goodyear, X. Yang, E. R. Angert and C. A. Batt, *Colloids Surf., B*, 2007, **57**, 161–173.
147 Z.-D. Gao, H.-F. Liu, C.-Y. Li and Y.-Y. Song, *Chem. Commun.*, 2013, **49**, 774–776.
148 G. Nie, A. D. Sheftel, S. F. Kim and P. Ponka, *Blood*, 2005, **105**, 2161–2167.
149 M. Hoppler, L. Meile and T. Walczyk, *Anal. Bioanal. Chem.*, 2008, **390**, 53–59.
150 H. Chen, S. Zhang, C. Xu and G. Zhao, *Chem. Commun.*, 2016, **52**, 7402–7405.
151 S. Yin, B. Zhang, J. Lin, Y. Liu, Z. Su and J. Bi, *Eng. Life Sci.*, 2021, **21**, 630–642.
152 B. Maity and T. Ueno, in *Protein Cages: Design, Structure, and Applications*, ed. T. Ueno, S. Lim and K. Xia, Springer US, New York, NY, 2023, pp. 135–145.
153 M. Liang, K. Fan, M. Zhou, D. Duan, J. Zheng, D. Yang, J. Feng and X. Yan, *Proc. Natl. Acad. Sci. U. S. A.*, 2014, **111**, 14900–14905.
154 T. Tan, H. Wang, H. Cao, L. Zeng, Y. Wang, Z. Wang, J. Wang, J. Li, S. Wang, Z. Zhang and Y. Li, *Adv. Sci.*, 2018, **5**, 1801012.
155 J. Zhang, D. Cheng, J. He, J. Hong, C. Yuan and M. Liang, *Nat. Protoc.*, 2021, **16**, 4878–4896.
156 K. K. W. Wong and S. Mann, *Adv. Mater.*, 1996, **8**, 928–932.
157 K. Iwahori and I. Yamashita, *J. Phys.: Conf. Ser.*, 2007, **61**, 492.
158 K. Iwahori, K. Yoshizawa, M. Muraoka and I. Yamashita, *Inorg. Chem.*, 2005, **44**, 6393–6400.
159 M. Peskova, L. Ilkovics, D. Hynek, S. Dostalova, E. M. Sanchez-Carnerero, M. Remes, Z. Heger and V. Pekarik, *J. Colloid Interface Sci.*, 2019, **537**, 20–27.
160 M. G. Walls, C. Cao, K. Yu-Zhang, J. Li, R. Che and Y. Pan, *Microsc. Microanal.*, 2013, **19**, 835–841.
161 U. B. Sleytr, B. Schuster, E.-M. Egelseer and D. Pum, *FEMS Microbiol. Rev.*, 2014, **38**, 823–864.
162 U. B. Sleytr, P. Messner, D. Pum and M. Sára, *Angew. Chem., Int. Ed.*, 1999, **38**, 1034–1054.
163 U. B. Sleytr, *J. Ultrastruct. Res.*, 1976, **55**, 360–377.
164 D. Pum, J. L. Toca-Herrera and U. B. Sleytr, *Int. J. Mol. Sci.*, 2013, **14**, 2484–2501.
165 A. Blecha, K. Zarschler, K. A. Sjollema, M. Veenhuis and G. Rödel, *Microb. Cell Fact.*, 2005, **4**, 28.
166 P. Messner, D. Pum and U. B. Sleytr, *J. Ultrastruct. Mol. Struct. Res.*, 1986, **97**, 73–88.
167 M. Jarosch, E. M. Egelseer, C. Huber, D. Moll, D. Mattanovich, U. B. Sleytr and M. Sára, *Microbiology*, 2001, **147**, 1353–1363.

168 U. Queitsch, C. Hamann, F. Schäffel, B. Rellinghaus, L. Schultz, A. Blüher and M. Mertig, *J. Phys. Chem. C*, 2009, **113**, 10471–10476.
169 E. Valero, M. Martín, N. Gálvez, P. Sánchez, J. Raff, M. L. Merroun and J. M. Dominguez-Vera, *Inorg. Chem.*, 2015, **54**, 6758–6762.
170 C. B. Maliakkal, E. K. Mårtensson, M. U. Tornberg, D. Jacobsson, A. R. Persson, J. Johansson, L. R. Wallenberg and K. A. Dick, *ACS Nano*, 2020, **14**, 3868–3875.
171 M. Abdolirad, R. Khalilzadeh and M. Alijanianzadeh, *Superlattices Microstruct.*, 2018, **120**, 370–376.
172 S. Abe, T. T. Pham, H. Negishi, K. Yamashita, K. Hirata and T. Ueno, *Angew. Chem.*, 2021, **133**, 12449–12453.
173 A. A. Kermani, *FEBS J.*, 2021, **288**, 5788–5804.
174 Z. E. R. Newby, I. I. I. Joseph, D. O'Connel, F. Gruswitz, F. A. Hays, W. E. C. Harries, I. M. Harwood, J. D. Ho, J. K. Lee, D. F. Savage, L. J. W. Miercke and R. Stroud, *Nat. Protoc.*, 2009, **4**, 619.
175 N. C. Seeman, *J. Theor. Biol.*, 1982, **99**, 237–247.
176 A. R. Ward and C. D. Snow, *Curr. Opin. Struct. Biol.*, 2020, **60**, 85–92.
177 A. R. Orun, E. T. Shields, S. Dmytriw, A. Vajapayajula, C. K. Slaughter and C. D. Snow, *ACS Nano*, 2023, **17**, 13110–13120.
178 H. Komori, F. Matsunaga, Y. Higuchi, M. Ishiai, C. Wada and K. Miki, *EMBO J.*, 1999, **18**, 4597–4607.
179 S. Karamikamkar, E. P. Yalcintas, R. Haghniaz, N. R. de Barros, M. Mecwan, R. Nasiri, E. Davoodi, F. Nasrollahi, A. Erdem, H. Kang, J. Lee, Y. Zhu, S. Ahadian, V. Jucaud, H. Maleki, M. R. Dokmeci, H.-J. Kim and A. Khademhosseini, *Adv. Sci.*, 2023, **10**, 2204681.
180 L. Wan, Q. Chen, J. Liu, X. Yang, J. Huang, L. Li, X. Guo, J. Zhang and K. Wang, *Biomacromolecules*, 2016, **17**, 1543–1550.
181 J. Tang, X. Jia, Q. Li, Z. Cui, A. Liang, B. Ke, D. Yang and C. Yao, *Proc. Natl. Acad. Sci. U. S. A.*, 2023, **120**, e2303822120.
182 Y. Yuan and N. Solin, *ACS Appl. Bio Mater.*, 2022, **5**, 3360–3370.
183 D. Lovskaya, A. Bezchasnyuk, M. Mochalova, P. Tsygankov, A. Lebedev, Y. Zorkina, E. Zubkov, A. Ochneva, O. Gurina, A. Silantyev, A. Majouga and N. Menshutina, *Gels*, 2022, **8**, 765.
184 Y. A. Pardo, K. G. Yancey, D. S. Rosenwasser, D. M. Bassen, J. T. Butcher, J. E. Sabin, M. Ma, S. Hamada and D. Luo, *Mater. Today*, 2022, **53**, 98–105.
185 J. D. Stuart, D. A. Hartman, L. I. Gray, A. A. Jones, N. R. Wickenkamp, C. Hirt, A. Safira, A. R. Regas, T. M. Kondash, M. L. Yates, S. Driga, C. D. Snow and R. C. Kading, *PNAS Nexus*, 2022, **1**, pgac190.
186 A. P. Kiseleva, P. V. Krivoshapkin and E. F. Krivoshapkina, *Front. Chem.*, 2020, **8**, 554.
187 T. B. Aigner, E. DeSimone and T. Scheibel, *Adv. Mater.*, 2018, **30**, 1704636.
188 S. G. Wise, S. M. Mithieux and A. S. Weiss, *Adv. Protein Chem. Struct. Biol.*, 2009, **78**, 1–24.
189 S. Zhao, X. Ye, X. Dai, X. Wang, S. Yu and B. Zhong, *PLoS One*, 2023, **18**, e0282533.
190 R. Balu, N. K. Dutta, A. K. Dutta and N. R. Choudhury, *Nat. Commun.*, 2021, **12**, 149.
191 R. Zeng, K. Tang, H. Tian and Y. Pei, *J. Polym. Sci.*, 2024, **62**(6), 998.
192 H. A. Tran, T. T. Hoang, A. Maraldo, T. N. Do, D. L. Kaplan, K. S. Lim and J. Rnjak-Kovacina, *Mater. Today*, 2023, **65**, 244–259.
193 W. Fang, R. Fan, A. S. Aranko, M. Hummel and H. Sixta, *ACS Sustainable Chem. Eng.*, 2023, **11**, 14807–14815.
194 L. F. Hartje, D. A. Andales, L. P. Gintner, L. B. Johnson, Y. V. Li and C. D. Snow, *Crystals*, 2023, **13**(2), 352.
195 N. J. Culbert, M. Kaiser, N. Venter, M. J. B. Vreysen, J. R. L. Gilles and J. Bouyer, *Parasites Vectors*, 2020, **13**, 192.
196 J. B. Silver, *Mosquito Ecology: Field Sampling Methods*, Springer, Dordrecht, 3rd edn, 2007.
197 J. L. Watson, D. Juergens, N. R. Bennett, B. L. Trippe, J. Yim, H. E. Eisenach, W. Ahern, A. J. Borst, R. J. Ragotte, L. F. Milles, B. I. M. Wicky, N. Hanikel, S. J. Pellock, A. Courbet, W. Sheffler, J. Wang, P. Venkatesh, I. Sappington, S. V. Torres, A. Lauko, V. De Bortoli, E. Mathieu, S. Ovchinnikov, R. Barzilay, T. S. Jaakkola, F. DiMaio, M. Baek and D. Baker, *Nature*, 2023, **620**, 1089–1100.
198 A. Madani, B. Krause, E. R. Greene, S. Subramanian, B. P. Mohr, J. M. Holton, J. L. Olmos, C. Xiong, Z. Z. Sun, R. Socher, J. S. Fraser and N. Naik, *Nat. Biotechnol.*, 2023, **41**, 1099–1106.
199 J. B. Ingraham, M. Baranov, Z. Costello, K. W. Barber, W. Wang, A. Ismail, V. Frappier, D. M. Lord, C. Ng-Thow-Hing, E. R. Van Vlack, S. Tie, V. Xue, S. C. Cowles, A. Leung, J. V. Rodrigues, C. L. Morales-Perez, A. M. Ayoub, R. Green, K. Puentes, F. Oplinger, N. V. Panwar, F. Obermeyer, A. R. Root, A. L. Beam, F. J. Poelwijk and G. Grigoryan, *Nature*, 2023, **623**, 1070–1078.
200 Z. Li, S. Wang, U. Nattermann, A. K. Bera, A. J. Borst, M. Y. Yaman, M. J. Bick, E. C. Yang, W. Sheffler, B. Lee, S. Seifert, G. L. Hura, H. Nguyen, A. Kang, R. Dalal, J. M. Lubner, Y. Hsia, H. Haddox, A. Courbet, Q. Dowling, M. Miranda, A. Favor, A. Etemadi, N. I. Edman, W. Yang, C. Weidle, B. Sankaran, B. Negahdari, M. B. Ross, D. S. Ginger and D. Baker, *Nat. Mater.*, 2023, 1–8.
201 A. Gazizov, A. Lian, C. Goverde, S. Ovchinnikov and N. F. Polizzi, 2023, 2023.10.15.562410.